Coupling 3D peridynamics and high order 1D finite elements for the linear static analysis of solid beams and thin-walled reinforced structures

A. Pagani*, E. Carrera

Mul^2 Team
Department of Mechanical and Aerospace Engineering, Politecnico di Torino
Corso Duca degli Abruzzi 24, 10129 Torino, Italy.

Abstract: *Peridynamics is a non-local theory which has been successfully applied to solid mechanics and crack propagation problems over the last decade. This methodology, however, may bring to large computational calculations which can soon become unhandleable for many problems of practical interest. In this context, a technique to couple –in a global/local sense– 3D peridynamics with 1D high order finite elements is proposed. The refined finite elements employed in this work are based on the well-established Carrera Unified Formulation (CUF), which the previous literature has demonstrated to provide structural formulations with unprecedented accuracy and optimized computational efficiency. The coupling is realized by using Lagrange multipliers, that guarantee versatility and physical consistency as demonstrated by the numerical results, including the linear static analyses of solid and thin-walled beams as well as of a reinforced panel of aeronautic interest.*

Keywords: Carrera unified formulation, Higher-order beam theories; Peridynamics.

1 Introduction

The peridynamic (PD) theory is a continuum version of molecular dynamics and is due to the seminar work of Silling [1]. It assumes that a solid body is composed by material particles and each pair of those interacts if their distance is less than a prescribed material horizon of radius δ. In other words, peridynamics is a non-local theory and does not necessarily imply differentiability of the primary unknowns (i.e., displacements in the case under consideration) along the spatial coordinates. Based on integro-differential equations, PD allows -naturally- the description of discontinuous displacement fields. Mainly for this reason, this theory has acquired the interest of many researchers working on fracture mechanics, see [2].

Over the past two decades, peridynamics has been demonstrated to provide reliable results for many problems, including crack initiation and propagation in brittle materials [3, 4], fatigue and fracture of composites [5], as well as impact [6]. Nevertheless, it should be underlined that, if compared to classical elasticity and related well-established computational methods, e.g. the finite element method (FEM), peridynamic models may be affected by large

*Corresponding author. E-mail: alfonso.pagani@polito.it

computational demand, especially if fully 3D problems are considered and the assumptions for plain-stress or plain-strain do not hold. The reason is that PD is a non-local theory and, thus, results into numerical methodologies that make use of sparse, large, and generally not banded arrays. From a practical point of view and for problems of engineering interest, PD may be unfeasible.

In this context, current research is intended to provide coupled models in which FEM and PD domains coexist. In this manner, one may combine the advantages of the two technologies and possibly use PD in small regions of the structure where crack is likely to develop. Galvanetto *et al.* [7] showed that coupling FEM to PD is not as simple as sharing nodes between meshes with dissimilar discretization. In fact, in PD domains, prescribed displacements or loads must be applied through a finite volume rather than on a surface. Thus, the coupling must be done over a region that spans some length (typically the horizon) from the external surface. To solve this issue, the authors proposed a coupling technique in which PD bonds act only on peridynamic particles, whereas finite elements apply forces only on FE nodes.

Interestingly, Kilic and Madenci [8] developed a coupling method using an overlapping region in which both the peridynamic and the finite element equations are used to achieve an appropriate coupling between the two zones. Liu and Hong [9], in contrast, coupled PD and FEM sub-regions by using interface elements. In the papers of Seleson and co-workers, see for example [10], a strong coupling making use of blending functions was proposed. To avoid any arbitrary choice of artificial coupling parameters, Zaccariotto *et al.* [11] proposed an innovative coupling algorithm able to adaptively transform FEM nodes into PD particles. This method was demonstrated to be reliable for 1D, 2D, and 3D structures as well as for static and dynamic problems, including crack propagation.

Note that most of the methods available in the literature couple FEM and PD domains of consistent dimensionality. In other words, 1D FEM is coupled with a 1D PD grid, 2D plate finite elements are coupled with 2D plain-stress or plane-strains PD, and so on. In practice, many problems may require the use of a 3D peridynamic discretization in local regions of the structural domain, e.g. in the case of material inclusions or transverse crack in thick panels. In this case, the use of 3D FE-3D PD models is potentially prohibitive. In the present work, we propose the use of high order 1D finite elements to be coupled with 3D PD sub-regions. The 1D models employed are implemented in the framework of the Carrera Unified Formulation (CUF), according to which the displacement components are approximated with an arbitrary expansion of the generalized unknowns and through the use of opportune cross-sectional functions. The main advantage of CUF, is that the governing equations and consequently the finite element arrays of generally refined 1D models are expressed in terms of fundamental nuclei, which are invariant of the theory approximation order. Previous literature has demonstrated that 1D CUF can be applied indistinctly to many problems, including composite mechanics [12], progressive failure analysis [13], large displacements analysis [14], rotor-dynamics [15], and multi-field problems [16], among the others.

Coupled 3D PD-1D refined FE models are realized by considering two distinct domains. PD and FE sub-regions do not alter the stiffness of each other. Consistently, continuity among the interface is guaranteed by the use of Lagrange multipliers [17]. As a consequence, the coupled models have global-local capabilities, i.e. 3D PD can be literally embedded into the FE domain and only in the zones of interest. Moreover, thanks to CUF, which allows for the formulation of low to high order finite elements, the proposed algorithm is general and can be also applied to classical FEM models. However, when refined 1D elements are used, the coupled approach can provide a full 3D solution, both in terms of displacements and

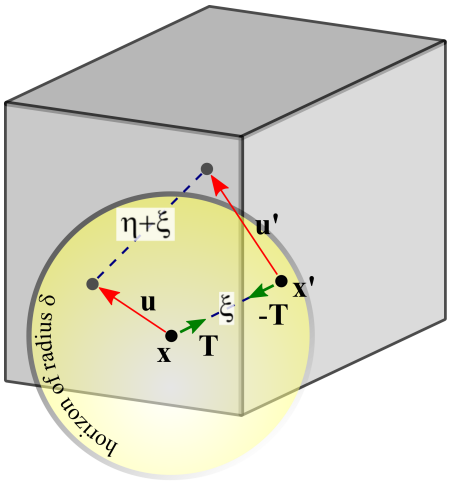

Figure 1: Particle $\boldsymbol{x}$ interacts by means of peridynamic forces with all particles within a circular (spherical) neighbourhood of radius δ (horizon). Every material particle $\boldsymbol{x}'$ is associated to a volume $V_{x'}$ and exerts a force (per unit of volume squared) $\boldsymbol{T}(\boldsymbol{\eta}, \boldsymbol{\xi})$ on the particle $\boldsymbol{x}$.

stress/strain fields.

The paper is organized as follows: Section 2 briefly introduces bond-based peridynamics along with an opportune meshless discretization of the problem equations; then, CUF-based 1D finite elements are discussed; the proposed coupling approach, making use of Lagrange multipliers, is detailed in Section 4; Next, some representative numerical results, including solid and thin-walled beams as well as a reinforced panel of aeronautic interest, are summarized; Finally, Section 6 outlines important conclusions.

2 Bond-based peridynamics

Figure 1 shows two connected particles $\boldsymbol{x}$ and $\boldsymbol{x}'$ in a solid region. In the following discussion, we denote the relative position of these two particles in the reference configuration by $\boldsymbol{\xi}$:

$$\boldsymbol{\xi} = \boldsymbol{x}' - \boldsymbol{x} \tag{1}$$

Assume that the two particles are displaced respectively by $\boldsymbol{u}$ and $\boldsymbol{u}'$, the relative displacement vector is given by $\boldsymbol{\eta}$:

$$\boldsymbol{\eta} = \boldsymbol{u}' - \boldsymbol{u} \tag{2}$$

Note that $\boldsymbol{\eta} + \boldsymbol{\xi}$ represents the current relative position vector between the particles.

The physical interaction between the particles at $\boldsymbol{x}$ and $\boldsymbol{x}'$ is called a *bond*, which extends over a finite distance. Bonded particle $\boldsymbol{x}'$ exerts a force $\boldsymbol{T}(\boldsymbol{\eta}, \boldsymbol{\xi})$ on particle $\boldsymbol{x}$. $\boldsymbol{T}$ is a pairwise force (per unit volume squared) function; is symmetric, i.e. $\boldsymbol{T}(\boldsymbol{\eta}, \boldsymbol{\xi}) = \boldsymbol{T}(-\boldsymbol{\eta}, -\boldsymbol{\xi})$; and vanishes for $|\boldsymbol{\xi}| > \delta$.

According to the seminar work of Silling [1], the static equilibrium equation of particle $\boldsymbol{x}$ takes the following integral form:

$$\int_{\mathcal{H}_x} \boldsymbol{T}(\boldsymbol{\eta}, \boldsymbol{\xi}) \, \mathrm{d}V_{x'} + \boldsymbol{b}(\boldsymbol{x}) = \boldsymbol{0} \tag{3}$$

where $\mathcal{H}_x$ is a neighbourhood of $\boldsymbol{x}$ and $\boldsymbol{b}$ is a prescribed body force density field. For simplicity, it is usually assumed that the bond force $\boldsymbol{T}$ depends only on the *bond stretch*, defined by the

following scalar variable:

$$s = \frac{|\boldsymbol{\eta} + \boldsymbol{\xi}| - |\boldsymbol{\xi}|}{|\boldsymbol{\xi}|} \tag{4}$$

In the prototype micro elastic brittle material (PMB) proposed by Silling [1], the stretch s and the pairwise force function $\boldsymbol{T}$ are related by:

$$\boldsymbol{T} = c\, s\, \frac{\boldsymbol{\eta} + \boldsymbol{\xi}}{|\boldsymbol{\eta} + \boldsymbol{\xi}|} \cong c\, s\, \frac{\boldsymbol{\xi}}{|\boldsymbol{\xi}|} \tag{5}$$

where c is the bond stiffness and the stretch direction $\boldsymbol{n} = \frac{\boldsymbol{\eta}+\boldsymbol{\xi}}{|\boldsymbol{\eta}+\boldsymbol{\xi}|}$ has been simplified as $\frac{\boldsymbol{\xi}}{|\boldsymbol{\xi}|}$, which is valid in case of small displacements.

Considerations about the elastic deformation energy allow the definition of the bond stiffness c in terms of the Young modulus E and the horizon radius δ. In the case of 3D elastic bodies, as in this work, one has [18]

$$c = \frac{12E}{\pi\delta^4} \tag{6}$$

Because of the hypotheses made, the Poisson ratio is constrained to $\nu = 1/4$ in the case of 3D bond-based peridynamics. This limitation has been removed in the state-based peridynamics [19].

2.1 Discretization

The elastic body is discretized into a grid of nodes, each with a known volume. After discretization, the static equilibrium integral equation (Eq. (3)) of the current node $\boldsymbol{x}_i$ can be given in a form of summation:

$$\sum_{j=1}^{N_{\mathcal{H}_i}} \boldsymbol{T}_{ij}\, V_j + \boldsymbol{b}_i = 0 \tag{7}$$

where $N_{\mathcal{H}_i}$ is the number of family nodes of $\boldsymbol{x}_i$ and V_j is the volume of particle $\boldsymbol{x}_j$. Note that this method is proposed as a meshfree scheme by Silling and Askari [2] in the sense that there are no elements or other geometrical connections between the nodes. In the proposed work, $V_j = \Delta x^3$, where Δx is the grid spacing, which is assumed to be constant. However, in order to consider the volume reduction of a node which has an intersection with the horizon boundary, a volume reduction scheme is introduced as in [20].

After linearization (Eq. (5)) and in the case of homogeneous media, Eq. (7) reads

$$\sum_{j=1}^{N_{\mathcal{H}_i}} \boldsymbol{C}(\boldsymbol{x}_j - \boldsymbol{x}_i)\,(\boldsymbol{u}_j - \boldsymbol{u}_i)\, V_j + \boldsymbol{b}_i = 0 \tag{8}$$

where $\boldsymbol{C}$ is the material's *micromodulus function*, whose value is a second-order tensor given by

$$\boldsymbol{C}(\boldsymbol{\xi}) = \frac{\partial \boldsymbol{T}}{\partial \boldsymbol{\eta}}(\boldsymbol{0}, \boldsymbol{\xi}) = c\frac{\boldsymbol{\xi}\boldsymbol{\xi}^T}{|\boldsymbol{\xi}|^3} \tag{9}$$

Observe that multiplying Eq. (8) by V_i leads to an equilibrium equation identical in form to that of finite element analysis [21]

$$\sum_{j=1}^{N_{\mathcal{H}_i}} \boldsymbol{C}(\boldsymbol{x}_j - \boldsymbol{x}_i)\,(\boldsymbol{u}_j - \boldsymbol{u}_i)\, V_i V_j + \boldsymbol{b}_i V_i = 0 \tag{10}$$

or

$$\boldsymbol{K}^{PD}\boldsymbol{U}^{PD} = \boldsymbol{F}^{PD} \tag{11}$$

3 High order 1D theories based on classical elasticity

The stiffness matrix of Eq. (11) is sparse, generally not banded. Moreover, due to the nonlocal nature of peridynamics, and depending on the horizon radius, the computational costs may result prohibitive, especially if structures with dimensions of engineering interest are analysed. To overcome this issue, researchers are actively working to couple peridynamics with finite elements based on classical elasticity. In this context, 3D peridynamics is coupled with 1D finite elements based on the Carrera Unified Formulation (CUF), which is a well-known methodology to generate higher order theories with enhanced accuracy [22].

In the domain of CUF, the 3D displacement field of a solid beam with main dimension along the y-axis, can be expressed as a generic expansion of the *generalized* displacements $\boldsymbol{u}_\tau(y)$:

$$\boldsymbol{u}(x,y,z) = F_\tau(x,z)\boldsymbol{u}_\tau(y), \qquad \tau = 1,2,....,M \tag{12}$$

where F_τ represent functions of the coordinates x and z on the cross-section, M stands for the number of the terms used in the expansion, and the repeated subscript τ indicates summation. The choice of F_τ determines the class of the 1D CUF model.

In the case of Taylor Expansion (TE) models, as an example, the generalized displacements are expanded around the beam axis by means of a Maclaurin polynomial of truncated order N, see [23]. In other words, F_τ functions are polynomials of the type $x^i z^j$ in the case of TE CUF models. For reasons of completeness, the full 3D displacement field of a quadratic ($N = 2$) TE beam model (TE2) is given in the following:

$$\begin{aligned}
u_x(x,y,z) &= u_{x_1}(y) + x\ u_{x_2}(y) + z\ u_{x_3}(y) + x^2\ u_{x_4}(y) + xz\ u_{x_5}(y) + z^2\ u_{x_6}(y)\\
u_y(x,y,z) &= u_{y_1}(y) + x\ u_{y_2}(y) + z\ u_{y_3}(y) + x^2\ u_{y_4}(y) + xz\ u_{y_5}(y) + z^2\ u_{y_6}(y)\\
u_z(x,y,z) &= u_{z_1}(y) + x\ u_{z_2}(y) + z\ u_{z_3}(y) + x^2\ u_{z_4}(y) + xz\ u_{z_5}(y) + z^2\ u_{z_6}(y)
\end{aligned} \tag{13}$$

Note that: (1) TE models are hierarchical; (2) In the case of a TE model of order N, the number of expansion terms is $M = (N+1)(N+2)/2$; (3) The classical beam theories (Euler Bernoulli and Timoshenko theories) are particular cases of the linear CUF TE model (TE1). This class of CUF models has been widely employed in the recent literature and in different engineering disciplines, see [24, 15]

TE CUF-based models have been demonstrated to be very efficient and effective for a wide range of problems. Nevertheless, they may be affected by inaccuracies when very short beams are considered (the TE expansion become inaccurate for cross-sectional points laying far from the beam axis) or when complex structural assemblies are considered, e.g. in the case of reinforced thin-walled structures, see [25]. For this class of structures, Lagrange Expansion (LE) models can be employed. LE beam theories, in fact, are based on the use Lagrange-type polynomials to expand the generalized displacements on the beam section domain, F_τ. The cross-section physical surface is discretize into a number of expansion sub-domains, whose polynomial degree depends on the type of Lagrange expansion employed. Three-node linear L3, four-node bilinear L4, nine-node quadratic L9, and sixteen-node cubic L16 beam models have been developed in the framework of CUF. For the sake of brevity, their explicit kinematics is not included here, but they can be found in Carrera and Petrolo [26]. For instance, the 3D displacement field of the quadratic L9 beam model reads:

$$\begin{aligned}
u_x(x,y,z) &= F_1(x,z)\ u_{x_1}(y) + F_2(x,z)\ u_{x_2}(y) + F_3(x,z)\ u_{x_3}(y) + ... + F_9(x,z)\ u_{x_9}(y)\\
u_y(x,y,z) &= F_1(x,z)\ u_{y_1}(y) + F_2(x,z)\ u_{y_2}(y) + F_3(x,z)\ u_{y_3}(y) + ... + F_9(x,z)\ u_{y_9}(y)\\
u_z(x,y,z) &= F_1(x,z)\ u_{z_1}(y) + F_2(x,z)\ u_{z_2}(y) + F_3(x,z)\ u_{z_3}(y) + ... + F_9(x,z)\ u_{z_9}(y)
\end{aligned} \tag{14}$$

where F_1,...,F_9 form a usual quadratic Lagrange polynomial set. The main feature of LE models is that they make use of local expansions of pure displacement variables, being these arbitrary placed over the cross-section surface. This characteristic enables to capture complex 3D-like solutions at a global-local scale and to increase the accuracy of the solution in particular zones of interest. Recently, LE beam models have been employed for the component-wise analysis of composite laminates at various scales [27, 13], aerospace structures [28], and civil constructions [29].

3.1 Finite element approximation

Independently of the nature of the refined 1D theory adopted, the generalized displacements can be approximated along the beam axis by discretizing the 1D support with finite elements (FEs) to have:

$$\boldsymbol{u}_\tau(y) = N_i(y)\, \boldsymbol{u}_{\tau i}, \qquad i = 1, 2, ..., p+1 \tag{15}$$

In Eq. (15), i stands for summation and the generalized displacements are described as a function of the unknown nodal vector, $\boldsymbol{u}_{\tau i}$, and the 1D shape functions, N_i. In the case of classical Lagrangian shape functions, p is the polynomial order of the approximation of the single finite element and $p+1$ is the number of nodes per elements.

The main advantage of using a compact notation as in Eqs. (12) and (15) is that the governing equations and the FE arrays can be formulated in a unified and hierarchical manner, which is affected neither by the choice of the theory of structure, represented by F_τ, nor by the FE shape functions N_i. For instance, in the case of linear elastic, static problems, the governing equations can be obtained from the principle of virtual work, which states that:

$$\delta L_{\text{int}} = \delta L_{\text{ext}} \tag{16}$$

where δ is the virtual variation, L_{int} is the work of the internal strain energy, and L_{ext} is the work of the external forces. Now, the internal work reads:

$$\delta L_{\text{int}} = \int_l \int_\Omega \delta \boldsymbol{\epsilon}^T \boldsymbol{\sigma} \, \mathrm{d}\Omega \, \mathrm{d}y \tag{17}$$

where l is the length of the beam and Ω represents the surface of cross-section domain. In Eq. (17), $\boldsymbol{\sigma}$ and $\boldsymbol{\epsilon}$ are the vectors of the 3D stresses and strain components. By substituting the constitutive and geometric equations along with Eqs. (12) and (15), the expression of the internal work can be rewritten in a compact manner as follows:

$$\delta L_{\text{int}} = \delta \boldsymbol{u}_{\tau i}^T \mathbf{K}^{\tau s i j} \mathbf{u}_{s j} \tag{18}$$

where $\mathbf{K}^{\tau s i j}$ represents the 3×3 fundamental nucleus of the element stiffness matrix of the arbitrarily refined 1D beam theory. In the case of homogeneous isotropic material, the components of $\mathbf{K}^{\tau s i j}$ are

$$\begin{aligned} K_{\alpha\alpha}^{\tau s i j} &= (\lambda + 2G) \int_l N_i \, N_j \, \mathrm{d}y \int_\Omega F_{\tau,x} F_{s,x} \, d\Omega + G \int_l N_i \, N_j \, \mathrm{d}y \int_\Omega F_{\tau,z} F_{s,z} \, d\Omega + \\ &\quad + G \int_l N_{i,y} \, N_{j,y} \, \mathrm{d}y \int_\Omega F_\tau F_s \, d\Omega \\ K_{\alpha\beta}^{\tau s i j} &= \lambda \int_l N_i \, N_{j,y} \, \mathrm{d}y \int_\Omega F_\tau F_{s,x} \, d\Omega + G \int_l N_{i,y} \, N_j \, \mathrm{d}y \int_\Omega F_{\tau,x} F_s \, d\Omega \end{aligned} \tag{19}$$

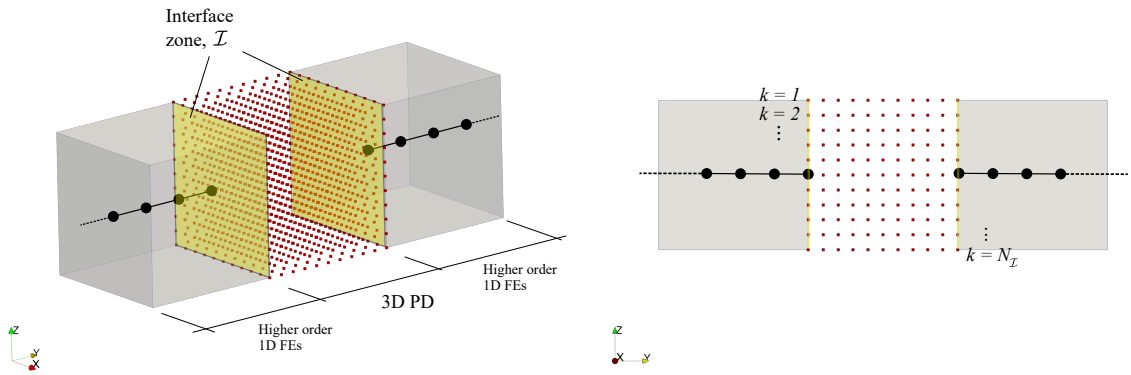

Figure 2: High order 1D finite elements are coupled with a 3D peridynamic region by using Lagrange multipliers. Given the interface zone $\mathcal{I}$, the Lagrangian Π_k of each particle $k \in \mathcal{I}$ is added to the FE-PD coupled (singular) system to satisfy the displacement continuity.

where λ and G are the two Lamé parameters. Moreover, $\alpha, \beta = x, y, z$; it is intended that all the nine components of the stiffness nucleus can be obtained by permutations from Eq. (19). Note that any refined beam model can be automatically formulated by expanding the fundamental nucleus within the stiffness matrix on τ, s, i, and j. Thus, once the stiffness matrix is expanded depending on the theory approximation order and assembled over the entire FE domain, Eq. (16) can be expressed as:

$$\boldsymbol{K}^{FE}\boldsymbol{U}^{FE} = \boldsymbol{F}^{FE} \tag{20}$$

where $\boldsymbol{U}^{FE}$ is the vector of the FE nodal unknowns and $\boldsymbol{F}^{FE}$ is the vector of external forces coming from the manipulation of δL_{ext}.

This section is not intended to be comprehensive, but gives essential notions useful for the derivation of a coupled high order 1D - 3D peridynamic model to be used in elastostatic problems. Readers interested in the FE derivation of CUF-based models are referred to Carrera *et al.* [30].

4 Coupling

Figure 2 shows a rectangular cross-section solid beam in a Cartesian reference system. A portion of the solid body is modelled by 3D peridynamics (peridynamic particles are denoted by red dots), whereas the rest of the domain is discretized by high order 1D elements. Neglecting for a moment any interface relation, the peridynamic region and the FEs can be modelled indipendently; Eqs. (11) and (20) are assembled in a weak sense to give the following system of linear algebraic equations:

$$\boldsymbol{K}\boldsymbol{U} = \boldsymbol{F}, \text{ i.e. } \begin{bmatrix} \boldsymbol{K}^{PD} & \boldsymbol{0} \\ \boldsymbol{0} & \boldsymbol{K}^{FE} \end{bmatrix} \begin{Bmatrix} \boldsymbol{U}^{PD} \\ \boldsymbol{U}^{FE} \end{Bmatrix} = \begin{Bmatrix} \boldsymbol{F}^{PD} \\ \boldsymbol{F}^{FE} \end{Bmatrix} \tag{21}$$

Note that the global stiffness matrix $\boldsymbol{K}$ of Eq. (21) is singular. Given an interface (contact) zone, denoted by $\mathcal{I}$ in the figure, between the peridynamic domain and the 1D FEs, Lagrange multipliers are used in this work to satisfy the congruence conditions on $\mathcal{I}$ and eliminate the singularity of $\boldsymbol{K}$.

For doing so, consider one single peridynamic particle k of the $N_{\mathcal{I}}$ particles laying on $\mathcal{I}$. The functional (Lagrangian) that has to be added to the original problem of Eq. (21) is:

$$\Pi_k = \boldsymbol{\lambda}_k^T \left(\boldsymbol{u}_k^{PD} - \boldsymbol{u}^{FE}(x_k, y_k, z_k) \right) \tag{22}$$

where $\boldsymbol{u}_k^{PD}$ is the displacement vector of PD particle k and $\boldsymbol{u}^{FE}(x_k, y_k, z_k)$ is the displacement field of the FE counterpart. $\boldsymbol{\lambda}_k$ is the three-component vector containing the Lagrange multipliers; they represent the forces to be applied to the system in order to satisfy continuity between the peridynamic particle and the FE approximation at k. After subtituting Eqs. (12) and (15) into Eq. (22), one has

$$\Pi_k = \boldsymbol{\lambda}_k^T \left(\boldsymbol{u}_k^{PD} - \boldsymbol{u}_{\tau i}^{FE} F_\tau(x_k, z_k) N_i(z_k) \right), \quad \tau = 1, ..., M, \quad i = 1, ..., p+1 \tag{23}$$

Equation (23) is, thus, expanded over τ and i to give, in a matrix form, the following expression:

$$\Pi_k = \boldsymbol{\lambda}_k^T \boldsymbol{B}_k \boldsymbol{U} \tag{24}$$

where $\boldsymbol{B}_k$ is the coupling matrix of particle k and its fundamental nucleus reads as:

$$\boldsymbol{B}_k^{\tau i} = \left(\delta_k - F_\tau(x_k, z_k) N_i(z_k) \right) \boldsymbol{I} \tag{25}$$

where $\boldsymbol{I}$ is the 3×3 identity matrix and δ_k is 1 for PD particle k and null otherwise.

After the Lagrangian of each particle $k \in \mathcal{I}$ is found and the total functional $\Pi = \sum_{k=1}^{N_{\mathcal{I}}} \Pi_k$ is calculated, the solution of the coupled problem is given by finding $\boldsymbol{U}$ and $\boldsymbol{\lambda}$ (Lagrange multipliers' vector of $3 \times N_{\mathcal{I}}$ components) from the following linear system:

$$\begin{cases} \boldsymbol{K}\boldsymbol{U} + \dfrac{\partial \Pi}{\boldsymbol{U}} = \boldsymbol{F} \\ \dfrac{\partial \Pi}{\boldsymbol{\lambda}} = 0 \end{cases} \tag{26}$$

or, equivalently,

$$\begin{bmatrix} \boldsymbol{K} & \boldsymbol{B}^T \\ \boldsymbol{B} & \boldsymbol{0} \end{bmatrix} \begin{Bmatrix} \boldsymbol{U} \\ \boldsymbol{\lambda} \end{Bmatrix} = \begin{Bmatrix} \boldsymbol{F} \\ \boldsymbol{0} \end{Bmatrix} \tag{27}$$

where $\boldsymbol{B}$ is the final coupling matrix coming from the assembly of $\boldsymbol{B}_k$'s.

For further readings about the use of Lagrange multipliers for coupling structural models with inconsistent kinematics, interested readers are referred to [17, 31]. Note that the proposed methodology is valid for any 1D finite elements, including classical Euler-Bernoulli and Timoshenko models available in any finite element packages of commercial relevance. The main advantage of the proposed methodology is that FE and PD non-conforming grids can be coupled with ease. In other words, the grid spacing of the peridynamic domain does not play any role in the choice of the FE mesh size in the coupled problem. Furthermore, if 1D high order finite elements are used in conjunction with PD, one has the capability to describe the entire computational domain with 3D accuracy, although the computational costs are low if compared to a full 3D PD analysis. In this sense, the peridynamic region can be limited in those zones of the structure were it is strictly needed.

As it will be clear in the discussion of the numerical results, the only disadvantage of the method proposed in this research is that the interface zone $\mathcal{I}$ may be affected by softening issues, especially when 3D PD is coupled with high order FEs which take into account the cross-section deformability. However, this is a well-known problem of PD and coupled PD-FEM methods and can be partially overcome by using overlapping regions. This will be the subject of future studies although.

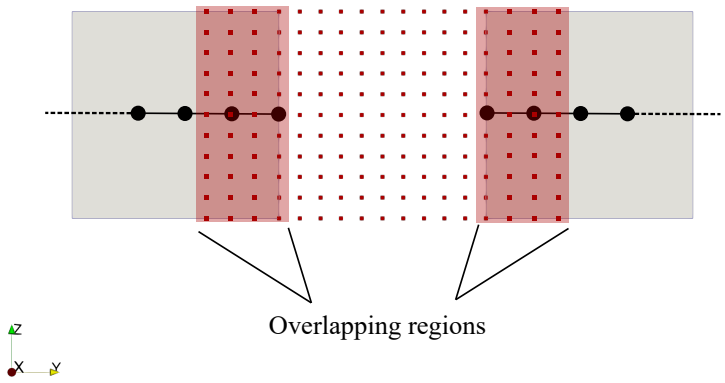

Figure 3: Overlapping regions between the peridynamic and finite element domain can be used to attenuate the softening issue at the interface $\mathcal{I}$.

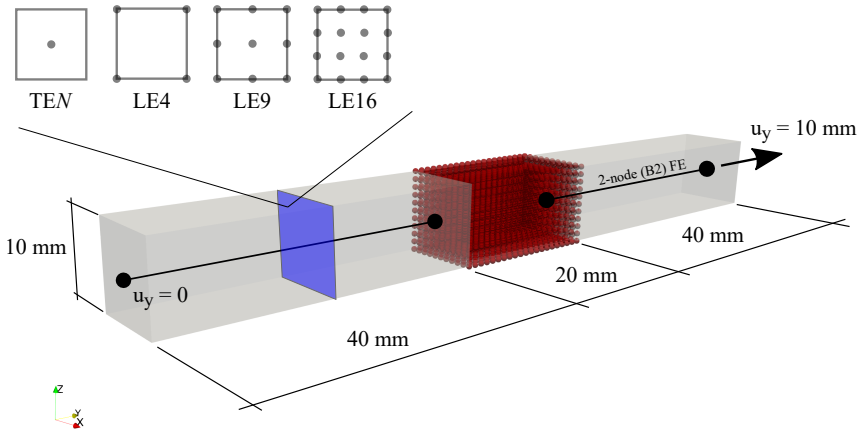

Figure 4: Square cross-section bar subjected to uniaxial tension. The peridynamic zone is discretized with a grid spacing $\Delta x = 1$ mm. The FE domains, instead, are modelled each with one single two-node (B2) linear element. The theory approximation of the FEs is varied from classical to high order LE.

5 Numerical results

5.1 Bar under uniaxial tension

In the first analysis case, we consider a 3D bar under uniaxial tension. Figure 4 shows geometry, boundary conditions and main modelling features. The bar has a square cross-section with side and length equal to 10 and 100 mm, respectively. The entire structure is made of a homogeneous isotropic material with Young modulus $E = 10$ GPa and $\nu = 0.25$. Peridynamics is used to model a small portion of the entire domain and a grid spacing of $\Delta x = 1$ mm is employed. In contrast, the horizon δ is varied. The remaining parts of the bar are modelled each with one single two-node (linear) 1D finite element, see Fig. 4. Thus, by using CUF, the kinematics (the theory of structure) associated with the FEs is varied from classical beam models (which are particular cases of TE1) to high order LE.

As a first result, Fig. 5 shows the deformed state of the bar under consideration. The model shown makes use of a bilinear L4 beam model (see Section 3) in the FE region, whereas

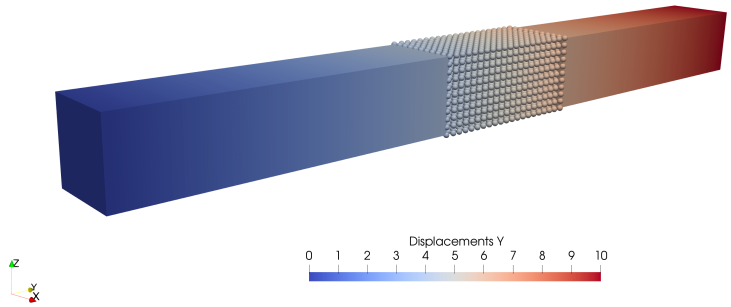

Figure 5: Deformed state of the square cross-section bar subjected to uniaxial tension. In this analysis case, the two 1D finite elements make use of a bilinear (L4) kinematics. The peridynamic zone has a horizon $\delta = 3$ mm.

Table 1: Value of the Poisson ratio calculated at the peridynamic zone of the bar under uniaxial traction. When using classical FE beam elements (TE1), the results are affected by errors because the FE cross-section is rigid and the displacements gradients in the PD zone are higher. The effect of the horizon is negligible.

Model	FE dof's	PD dof's	ν	% error
		$\delta = 2$ mm		
TE1-PD	36	7623	0.223	-10.8
L4-PD	48	7623	0.243	-2.8
L9-PD	108	7623	0.244	-2.4
		$\delta = 3$ mm		
TE1-PD	36	7623	0.261	4.4
L4-PD	48	7623	0.250	0.0
L9-PD	108	7623	0.251	0.4

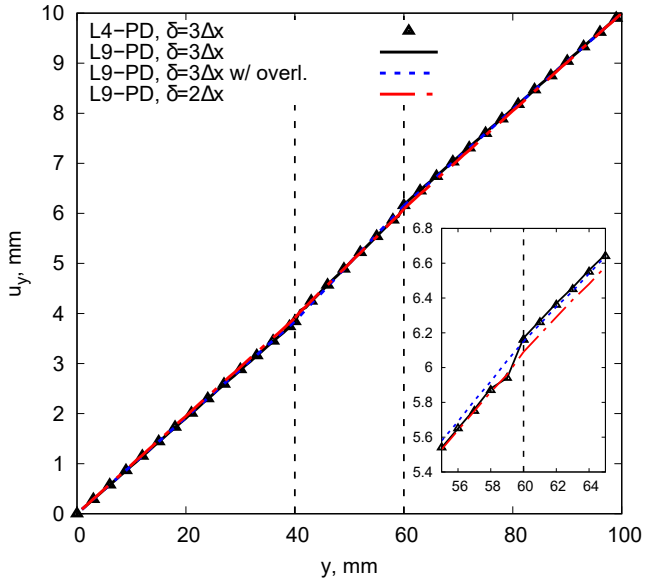

Figure 6: Axial displacement of the bar subjected to traction. FE-peridynamic interface may be subjected to distortions. In this analysis case, setting the PD horizon equal to twice the grid spacing or using overlapping zones helped to solve the issue.

a horizon $\delta = 3$ mm is used in the PD zone. To demonstrate the effect of the choice of the beam model and the horizon on the effectiveness of the present coupled approach, Table 1 is proposed. This table shows, for low to high order TE and LE beam models and different PD horizons, the value of the measured Poisson ratio ν and error with respect to expected value (0.25). It can be observed that, if classical and lower-order beam FE models are used (TE1 in Table 1), the Poisson ratio is misestimated. The reason is that the beam cross-section remains rigid in the entire FE domain in this case. In contrast, if high order FE elements are employed (e.g., L4 or L9), the 3D solution can be successfully recovered. Moreover, note from Table 1 that, for the case under consideration, the size of the FE problem is negligible with respect to the PD counterpart.

Figure 6 investigates the consistency of the solution at the interface boundary between the FE and PD zones. In detail, the figure shows the axial displacement u_y in the middle of the cross-section and along the entire length of the bar. It is demonstrated that the solution is not affected by the choice of the FE model utilized. On the other hand, it can be observed that some distortion is visible in correspondence of the transition zone. This is due to the well-known softening issues exhibited by peridynamics at the boundary regions and to the fact that PD and classical elasticity converge to different solutions. Nevertheless, from the analysis conducted, it is shown that this distortion at the contact interface can be attenuated by using a different value for the horizon radius. As an alternative, an overlapping zone can be used between the PD and FE zone. In this case, for example, the PD domain was considered to compenetrate the FE domain of a length along y equal to δ. Note that for all the numerical cases considered, these transition effects were scarcely visible and never affected the validity of the results. As a consequence, no artificial drawbacks have been employed hereinafter to better discuss the effectiveness of the method proposed.

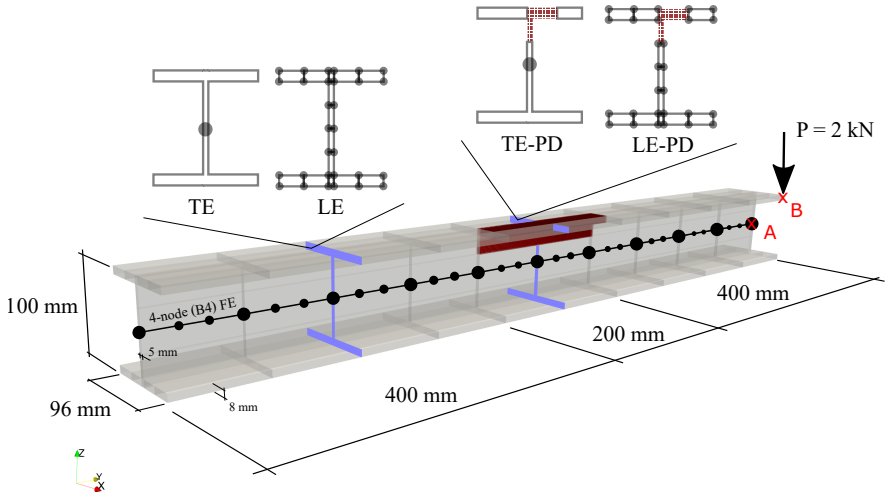

Figure 7: Cantilever I-section beam subjected to point load. The peridynamic zone, which has a grid spacing $\Delta x = 1$ mm and $\delta = 3\Delta x$, coexists with the FE domain. This latter is modelled with 10 four-node beam elements (B4). Note that the FE cross-section has a disconnected domain wherever PD lays.

5.2 I-section beam under bending and torsion

In the next numerical simulation we want to further highlight the 3D nature of the proposed approach. For this purpose, a cantilever I-section beam under bending and torsion is considered, see Fig. 7. The same problem was considered in previous works by Carrera and Pagani [32, 33], where geometrical characteristics, material properties and boundary conditions were also given along with reference solutions. In this section, we propose a coupled model in which peridynamics is used to discretize limited regions of the beam's aim and cap as shown in the figure. As in the previous case, the PD domain has a grid spacing of $\Delta x = 1$ mm and a horizon $\delta = 3$ mm. Note that the PD region is embedded into the FE domain itself, which is discretized with 10 four-node cubic (B4) 1D elements. For doing so, the cross-section of the 1D FEs vary along y; it is represented by a disconnected domain wherever PD lays, i.e. $400 \leq y \leq 600$ mm (see Fig. 7). Nevertheless, the CUF-based FEs make use of low-order to high-order TE and LE kinematics and the cross-section continuity and congruence is indistinctly satisfied by the use of Lagrange multipliers in the PD-FE zone $\mathcal{I}$.

Table 3 demonstrates the validity of the proposed methodology and compares the transverse displacements at points A and B from coupled PD-FE models with those from the previous literature. The reference solutions were obtained by using a commercial FE software tools (both a 2D-plate and a full 3D models are given) and CUF-based TE refined models based on a pure FE discretization. The reason of giving the displacements in two distinct points of the free end is that one can appreciate the ability of the refined CUF models of catching both bending and torsional behaviour of the beam under consideration. As a matter of fact, note that the PD-CUF models using high order TE and LE kinematics for the FEs are able to provide accurate results and all the coupled models proposed are coherent with the expected solutions. Furthermore, as 1D elements are used for the discretization of the FE zone, it can be observed that the number of degrees of freedom of the FE model is negligible with respect to those associated with PD. This is not the case when combining PD with 3D FEs. Finally, for completeness reason, we must underline that the TE reference solutions provided in Table 3 were obtained by discretizing the FE domain with 100 B2 finite elements. In this section instead, the same discretization is done with 10 B4 elements. This play a

Table 2: Vertical displacement components at the center of the free-end I-section and at the loading point. The results from the present PD-FE coupled method are compared with those from the literature. It is shown that refined beam FEs are needed to catch the bending-torsional behaviour. Nevertheless, for all the cases the coupled models are coherent with the expected solution.

Model	FE dof's	PD dof's	$-u_z$ [mm] @ Point A	$-u_z$ [mm] @ Point B
Reference solutions [32, 33]				
TE1	909*	-	0.964	0.964
TE4	4545	-	0.991	1.257
TE8	13635	-	0.997	1.649
TE14	36360	-	1.001	2.418
Nastran 2D	61000	-	1.006	2.437
Nastran 3D	355800	-	0.956	2.316
Present coupled PD-CUF models				
TE1-PD	279**	222507	0.967	0.981
TE4-PD	1395	222507	0.994	1.290
TE8-PD	4185	222507	1.002	1.846
TE14-PD	11160	222507	1.000	2.256
L9-PD	7911	222507	1.005	2.356

*100 B2 elements (101 FE nodes) are used in the TE ref. models.

**Present PD-CUF models employ 10 B4 elements instead (31 FE nodes).

role in the computation of the final number of dof's, but does not affect the validity of the analysis.

To further highlight the 3D nature of the coupled models proposed (3D in essence but not in the form), Fig. 8 shows the deformed shape of the I-section beam under consideration resulting from the low-order TE1-PD and high-order L9-PD models. It is clear that high accuracy can be reached if sufficiently rich kinematics is used for the 1D CUF-based FEs. Independently of the beam theories utilized in the FE zone, the 3D PD region is perfectly consistent with the formulation as demonstrated by Fig. 9, which shows a close detail on the deformed configuration.

Figure 10 shows the distribution of important stress components across the PD-FE interface plane at $y = 400$ mm. In fact, as demonstrated in the previous literature, given

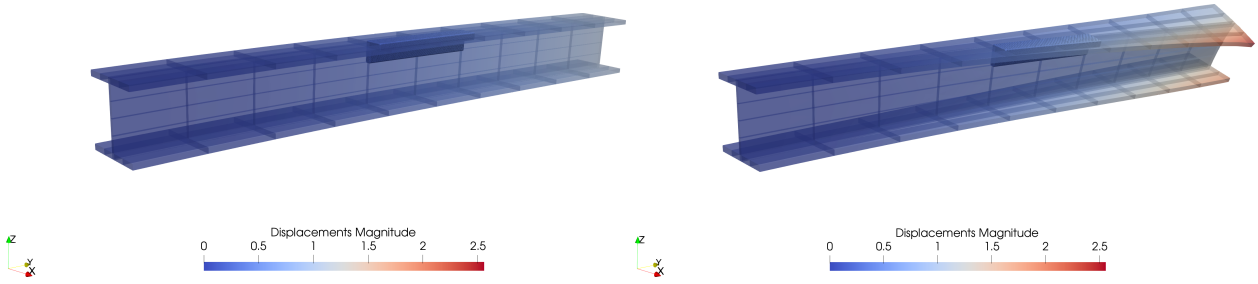

(a) TE1-PD (b) L9-PD

Figure 8: Deformed state of the I-section beam according to PD and low to high order FEs coupled models.

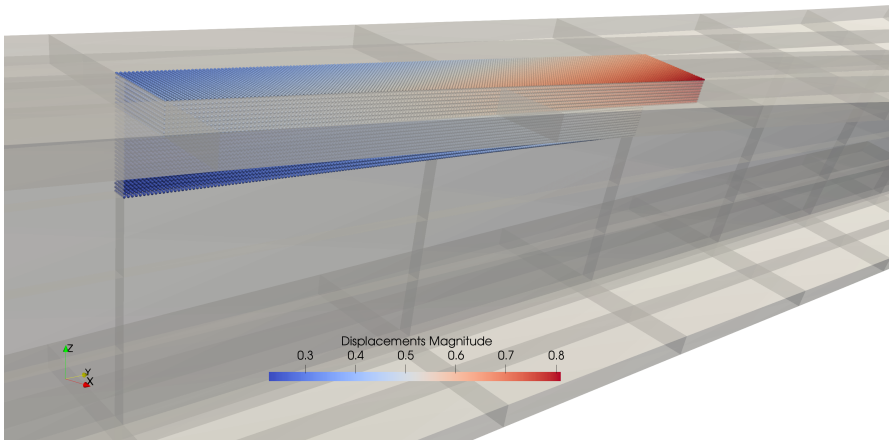

Figure 9: Detailed view of the deformed PD zone of the I-section beam according to coupled L9-PD model.

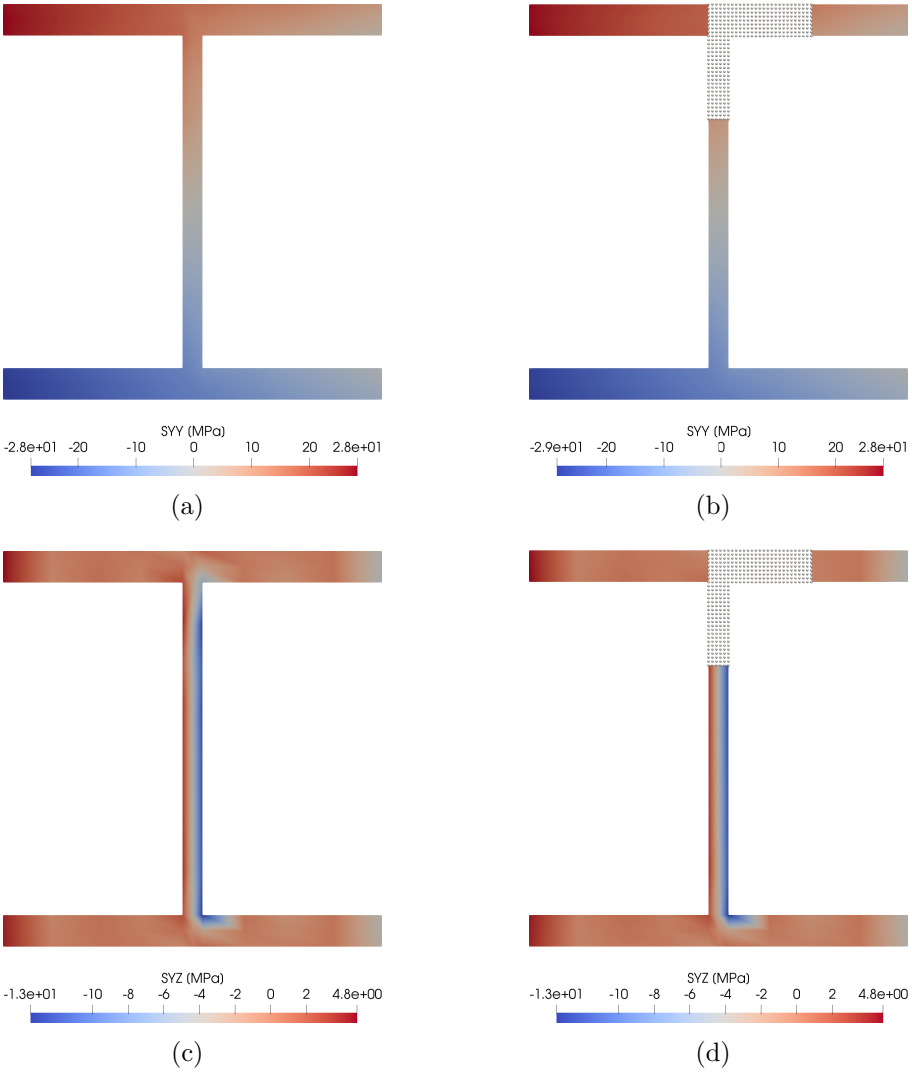

Figure 10: Distribution of axial stress (σ_{yy}, a-c) and transverse shear stress (σ_{yz}, b-d) across the FE-PD interface zone at $y = 400$ mm according to L9-PD model. The stress state is not affected by the PD interface.

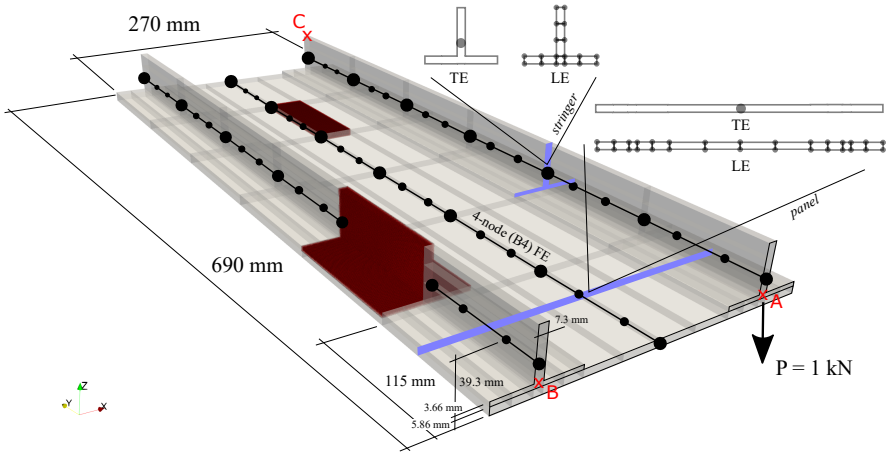

Figure 11: Reinforced panel subjected to point load. The panel and the stringers are modelled independently with six equally spaced 4-node beam elements (B4). Two different peridynamic zones are embedded in the model and they have a grid spacing $\Delta x = 1$ mm and $\delta = 3\Delta x$.

the displacements unknowns from Eq. (20), expanding with CUF (Eq. (12)) and using the 3D geometrical and constitutive relations, the 3D stress field can be recovered if sufficiently high kinematics is used although 1D FEs are employed, see [34, 13]. However, the important aspect here is that the stress state is not affected by PD and remains congruent also at the interface zone $\mathcal{I}$. This aspect may bring to important outcomes in fracture mechanics by coupled PD-CUF models.

5.3 Reinforced panel

As a final example, a reinforced panel of aerospace relevance is analysed to underline the possibility of the present method to study simple to complex geometries. Figure 11 shows the main geometric characteristics, the boundary conditions and the important modelling features. The entire stiffened panel is made of the same material of the first numerical example. The structure is composed by three main components (i.e. two stringers and one panel), each of which is modelled with higher-order 4-node beam elements, in a component-wise sense [25]. Two independent peridynamic regions are integrated into the FE model; i.e. a portion of the stringer and a small area of the panel as shown in Fig. 11. As in the previous cases, the PD zone is discretized in a meshless manner with a grid spacing of $\Delta x = 1$ mm and a horizon $\delta = 3$ mm.

Figure 12 demonstrates the deformed consideration of the structure under consideration and according to the proposed PD-CUF coupled approach. Furthermore, for completeness and validation purposes, Table 3 gives the vertical displacement values at two characteristics points (i.e., points A and B, see Fig. 11) and the maximum axial stress σ_{yy} at point C obtained via the present approach and reference solutions coming from a full FE analysis. Both the proposed results and the references make use of low to high-order CUF approximations in the FE domain, again to highlight the possibility to couple 3D peridynamics with any-order beam models.

The transverse displacement at point B and all along the panel span is given in a graphical form also in Fig. 13. In the figure, the solid line represent the reference, high-order L9 solution which make use of full FE discretization. Consistently, the present L9-PD perfectly matches the reference solution along the entire domain and also across the peridynamic stringer in-

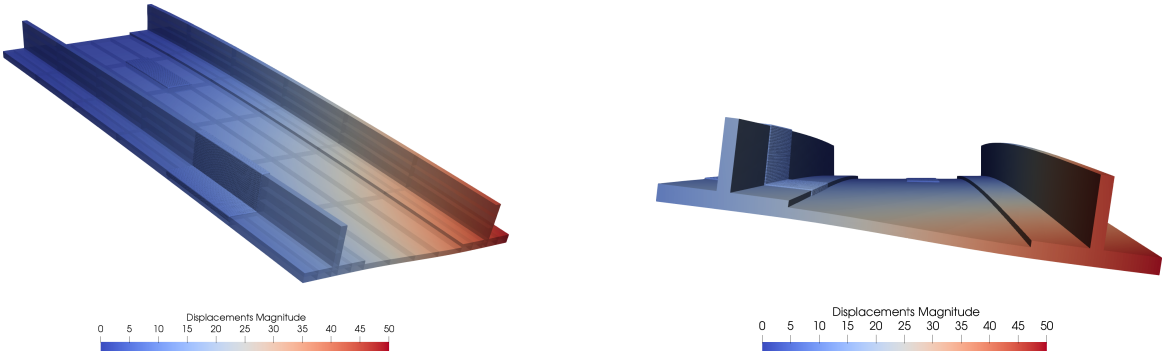

(a) (b)

Figure 12: Deformed state of the stiffened panel according to coupled L9-PD model.

Table 3: Vertical displacement components and maximum axial stress at different points of the reinforced panel. The results from the present PD-FE coupled method are compared with those from full FE approximations. For all the CUF theory approximation order, the coupled models are coherent with the expected solution.

Model	FE dof's	PD dof's	$-u_z$ [mm] @ Point A	$-u_z$ [mm] @ Point B	σ_{yy} [MPa] @ Point C
Reference solutions					
TE1	171	-	29.532	29.368	71.274
TE3	570	-	29.998	27.587	86.1674
TE5	1197	-	36.365	22.519	106.354
L9	9519	-	44.942	14.153	126.916
Present coupled PD-CUF models					
TE1-PD	171	312504	29.676	29.499	71.289
TE3-PD	570	312504	30.444	27.381	86.2379
TE5-PD	1197	312504	37.522	21.599	107.646
L9-PD	9261	312504	44.992	14.296	126.958

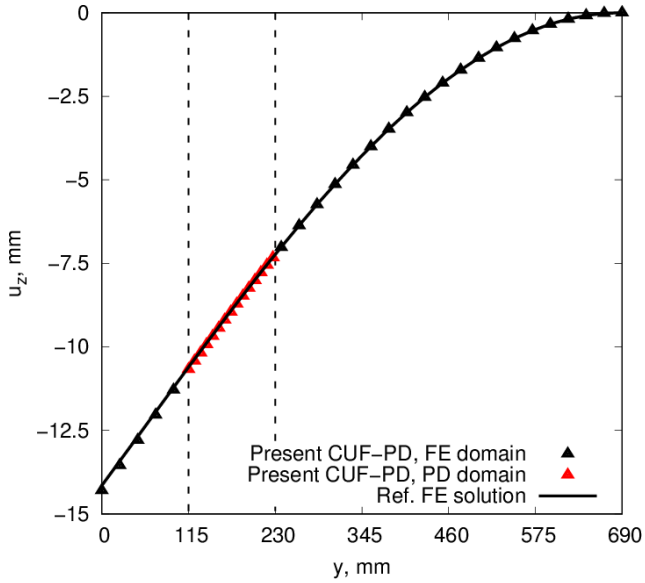

Figure 13: Transverse displacement of the stiffened panel at point B and all along the structure's span. Coupled L9-PD model is compared with a full FE model based on a high order L9 CUF beam theory. The coherence of the proposed method is demonstrated both in the FE and the PD domains.

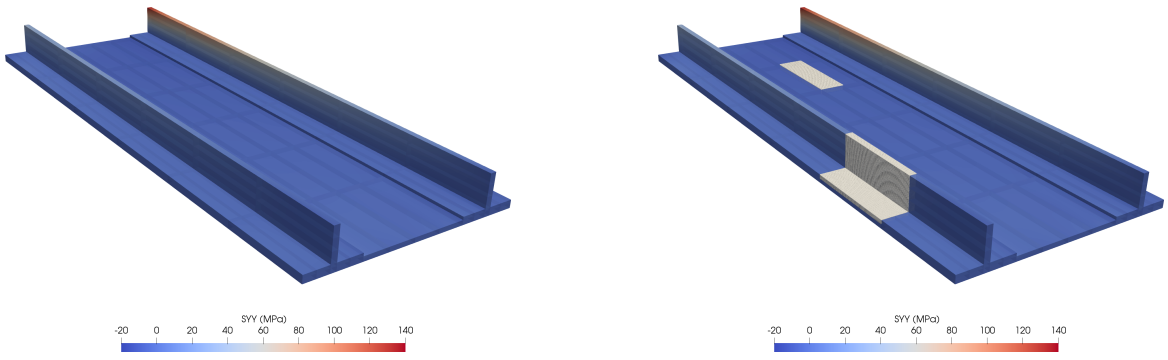

(a) L9 (b) L9-PD

Figure 14: Distribution of axial stress (σ_{yy}) according to the reference full FE L9 model and the present coupled L9-PD model.

terface. Finally, Fig. 14, which shows the 3D contour plot of the axial stress component σ_{yy}, demonstrates that multiple coupled PD-FE regions do not alter the consistency of the solution, even in terms of stress state.

6 Conclusions

This paper has discussed a novel technique to couple 3D peridynamics with high order 1D finite elements based on the Carrara Unified Formulation (CUF). The coupling technique is general and consistent, because it is based on the use of Lagrange multipliers, which have a clear physical meaning. Moreover, thanks to CUF, which provides any structural theory in a unified manner, 3D peridynamics can be coupled with 1D finite elements of arbitrary order, from classical to high order kinematics. Although, when refined finite elements are used, it is possible to obtain enhanced solutions with full 3D capabilities in which peridynamics is used in small zones of interest, in a global/local sense. The resulting coupled models have low computational efforts if compared to other 3D approaches and have been demonstrated to be effective for a wide range of structures, including solid beams and thin-walled constructions of aerospace relevance. The methodology will be extended to deal with localized progressive failure problems in future works.

7 Acknowledgements

This work is part of a project that has received funding from the European Research Council (ERC) under the European Union's Horizon 2020 research and innovation programme (Grant agreement No. 850437).
The authors would also like to acknowledge the DEVISU project, supported by the *Ministero dell'Istruzione, dell'Università e della Ricerca* research funding programme PRIN 2017.

References

[1] S. A. Silling. Reformulation of elasticity theory for discontinuities and long-range forces. *Journal of the Mechanics and Physics of Solids*, 48(1):175–209, 2000.

[2] S. A. Silling and E. Askari. A meshfree method based on the peridynamic model of solid mechanics. *Computers & Structures*, 83(17-18):1526–1535, 2005.

[3] Y.D. Ha and F. Bobaru. Characteristics of dynamic brittle fracture captured with peridynamics. *Engineering Fracture Mechanics*, 78(6):1156–1168, 2011.

[4] E. Madenci, K. Colavito, and N. Phan. Peridynamics for unguided crack growth prediction under mixed-mode loading. *Engineering Fracture Mechanics*, 167:34–44, 2016.

[5] Y. L. Hu and E. Madenci. Peridynamics for fatigue life and residual strength prediction of composite laminates. *Composite Structures*, 160:169–184, 2017.

[6] S.A. Silling, M.L. Parks, J.R. Kamm, O. Weckner, and M. Rassaian. Modeling shock-waves and impact phenomena with Eulerian peridynamics. *International Journal of Impact Engineering*, 107:47–57, 2017.

[7] U. Galvanetto, T. Mudric, A. Shojaei, and M. Zaccariotto. An effective way to couple FEM meshes and Peridynamics grids for the solution of static equilibrium problems. *Mechanics Research Communications*, 76:41–47, 2016.

[8] B. Kilic and E. Madenci. Coupling of peridynamic theory and the finite element method. *Journal of Mechanics of Materials and Structures*, 5(5):707–733, 2010.

[9] W. Liu and J.-W. Hong. A coupling approach of discretized peridynamics with finite element method. *Computer Methods in Applied Mechanics and Engineering*, 245-246(245):163–175, 2012.

[10] P. Seleson, S. Beneddine, and S. Prudhomme. A force-based coupling scheme for peridynamics and classical elasticity. *Computational Materials Science*, 66:34–49, 2013.

[11] M. Zaccariotto, T. Mudric, D. Tomasi, A. Shojaei, and U. Galvanetto. Coupling of FEM meshes with Peridynamic grids. *Computer Methods in Applied Mechanics and Engineering*, 330(330):471–497, 2018.

[12] E. Carrera and M. Petrolo. Refined one-dimensional formulations for laminated structure analysis. *AIAA Journal*, 50(1):176–189, 2012.

[13] I. Kaleel, M. Petrolo, E. Carrera, and A. M. Waas. Micromechanical progressive failure analysis of fiber-reinforced composite using refined beam models. *Journal of Applied Mechanics*, 85(2):021004, 2017.

[14] A. Pagani and E. Carrera. Unified formulation of geometrically nonlinear refined beam theories. *Mechanics of Advanced Materials and Structures*, 25(1):15–31, 2018.

[15] M. Filippi, A. Pagani, and E. Carrera. Accurate nonlinear dynamics and mode aberration of rotating blades. *Journal of Applied Mechanics*, 85:111004, 2018.

[16] E. Zappino, E. Carrera, S. Rowe, C. Mangeot, and H. Marques. Numerical analyses of piezoceramic actuators for high temperature applications. *Composite Structures*, 151:36–46, 2016.

[17] E. Carrera, A. Pagani, and M. Petrolo. Use of Lagrange multipliers to combine 1D variable kinematic finite elements. *Computers and Structures*, 129:194–206, 2013.

[18] A. Shojaei, M. Zaccariotto, and U. Galvanetto. Coupling of 2D discretized peridynamics with a meshless method based on classical elasticity using switching of nodal behaviour. *Engineering Computations*, 34(5):1334–1366, 2017.

[19] S. A Silling, M. Epton, O. Weckner, J. Xu, and E. Askari. Peridynamic states and constitutive modeling. *Journal of Elasticity*, 88(2):151–184, 2007.

[20] M. L. Parks, S. J. Plimpton, R. B. Lehoucq, and S. A. Silling. Peridynamics with LAMMPS: A user guide. Technical Report SAND 2008-1035, Sandia National Laboratories, 2008.

[21] R. W. Macek and S. A. Silling. Peridynamics via finite element analysis. *Finite Elements in Analysis and Design*, 43(15):1169–1178, 2007.

[22] E. Carrera, A. Pagani, M. Petrolo, and E. Zappino. Recent developments on refined theories for beams with applications. *Mechanical Engineering Reviews*, 2(2):1–30, 2015.

[23] E. Carrera, G. Giunta, and M. Petrolo. *Beam Structures: Classical and Advanced Theories*. John Wiley & Sons, 2011.

[24] A. G. de Miguel, A. Pagani, and E. Carrera. Higher-order structural theories for transient analysis of multi-mode lamb waves with applications to damage detection. *Journal of Sound and Vibration*, 457:139–155, 2019.

[25] E. Carrera, A. Pagani, and M. Petrolo. Classical, refined and component-wise theories for static analysis of reinforced-shell wing structures. *AIAA Journal*, 51(5):1255–1268, 2013.

[26] E. Carrera and M. Petrolo. Refined beam elements with only displacement variables and plate/shell capabilities. *Meccanica*, 47(3):537–556, 2012.

[27] E. Carrera, M. Maiarú, and M. Petrolo. Component-wise analysis of laminated anisotropic composites. *International Journal of Solids and Structures*, 49:1839–1851, 2012.

[28] E. Carrera, A. Pagani, and M. Petrolo. Component-wise method applied to vibration of wing structures. *Journal of Applied Mechanics*, 80(4):041012, 2013.

[29] E. Carrera, A. Pagani, and M. Petrolo. Refined 1D finite elements for the analysis of secondary, primary, and complete civil engineering structures. *Journal of Structural Engineering*, 141:04014123/1–14, 2015.

[30] E. Carrera, M. Cinefra, M. Petrolo, and E. Zappino. *Finite Element Analysis of Structures through Unified Formulation*. John Wiley & Sons, Chichester, West Sussex, UK, 2014.

[31] E. Carrera and A. Pagani. Analysis of reinforced and thin-walled structures by multiline refined 1D/beam models. *International Journal of Mechanical Sciences*, 75:278–287, 2013.

[32] E. Carrera and A. Pagani. Evaluation of the accuracy of classical beam fe models via locking-free hierarchically refined elements. *International Journal of Mechanical Sciences*, 100:169–179, 2015.

[33] E. Carrera and A. Pagani. Multi-line enhanced beam model for the analysis of laminated composite structures. *Composites: Part B*, 57:112–119, 2014.

[34] A. G. de Miguel, I. Kaleel, M. H. Nagaraj, A. Pagani, M. Petrolo, and E. Carrera. Accurate evaluation of failure indices of composite layered structures via various fe models. *Composites Science and Technology*, 167:174–189, 2018.